ARTICLES SCIENCE CHINA Materials

mater.scichina.com link.springer.com

Published online 21 March 2018 | https://doi.org/10.1007/s40843-017-9239-3
Sci China Mater 2018, 61(4): 516–524

SPECIAL ISSUE: Advances in Metallic Biomaterials

Corrosion resistance and cytocompatibility of Ti-20Zr-10Nb-4Ta alloy surface modified by a focused fiber laser

Xianda Xue[1], Chengpeng Ma[2], Hongjuan An[1], Yan Li[1,3*] and Yingchun Guan[2,4,5*]

ABSTRACT **The corrosion resistance and cytocompatibility of Ti-20Zr-10Nb-4Ta (TZNT) alloy modified by surface laser treatment were investigated. The scanning electron microscopy (SEM) measurements indicated that laser treatment on TZNT alloy generated groove morphologies with the width of ~40 μm and the depth of ~10 μm on the surface. The water contact angles along the groove direction decreased by 51% compared with that of the untreated alloy. The laser treatment promoted the oxidation of metallic Ti, Zr and Nb and produced more stable oxides on surface. The corrosion potential increased by 50% and corrosion current density decreased by 72% compared with that of the untreated alloy in the anodic polarization test for the alloy in Hank's solution at 37°C. This indicated the improvement of the corrosion resistance by laser treatment. The cytotoxicity testing results showed that the laser-treated TZNT alloy performed similar MC3T3-E1 cell viability compared with the untreated alloy. The cells displayed oriented growth along the groove direction due to the increased hydrophilicity. This novel material may be a new candidate in orthopedics and dentistry implantations fields.**

Keywords: laser, Ti-20Zr-10Nb-4Ta, corrosion resistance, cytocompatibility

INTRODUCTION

Due to the high strength to weight ratio, good corrosion resistance, and low density, commercially pure titanium (CP-Ti) and Ti-6Al-4V alloys have been widely used in biomedical fields such as orthopedics and dental implantations [1,2]. However, the disadvantages of CP-Ti and Ti-6Al-4V in clinical applications, e.g., very high Young's modulus, and toxic effects of V and Al elements, triggered the development of new bio-safe Ti alloys exhibiting low Young's modulus comparable to human bones [3,4,5]. Therefore, many Ti alloys made of nontoxic elements, e.g., Ti-Zr [6], Ti-Nb [7], Ti–13Nb–13Zr [8], Ti–35Nb–5Ta–7Zr [9], Ti–29Nb–13Ta–4.6Zr [10], and Ti-38.3Ta-22Zr-8.1Nb [11] alloys have been extensively investigated. These alloys exhibited low Young's modulus, good mechanical properties and excellent biocompatibility, showing the promise as new candidates in biomedical applications. Moreover, some of the recently developed Ti alloys such as Ti-19Zr-10Nb-1Fe [12,13] and Ti-20Zr-10Nb-4Ta [14] behaved good superelasticity and shape memory effects, and thus may challenge the Nitinol shape memory alloy in future clinical applications.

The laser surface treatment has been used to improve the mechanical properties, corrosion resistance and biocompatibility of Ti alloys [15,16]. On the one hand, a homogeneous microstructure and stable oxidation layer can be produced on the surface of the alloy owing to rapid re-solidification [17]. On the other hand, the heat energy localized at the surface level, leaving the bulk properties unaffected [18]. Lawrence *et al.* [19] indicated that the adhesiveness and proliferation of osteoblast cells can be enhanced when Ti-6Al-4V alloy was treated by a pulsed Nd : YAG laser, owing to the increased surface roughness and improved wettability. Chen *et al.* [20] reported that laser-treated microgrooves on Ti-6Al-4V alloy promoted

[1] School of Materials Science and Engineering, Beihang University, Beijing 100191, China
[2] School of Mechanical Engineering and Automation, Beihang University, Beijing 100191, China
[3] Beijing Advanced Innovation Centre for Biomedical Engineering, Beihang University, Beijing 100191, China
[4] National Engineering Laboratory of Additive Manufacturing for Large Metallic Components, Beihang University, Beijing 100191, China
[5] International Research Institute for Multidisciplinary Science, Beihang University, Beijing 100191, China
* Corresponding authors (emails: liyan@buaa.edu.cn (Li Y); guanyingchun@buaa.edu.cn (Guan Y))

cell adhesion with enhanced interactions between the focal adhesions and the extra-cellular matrix (ECM) proteins. Ulerich *et al.* [21] modified the Ti-6Al-4V surfaces by direct-write laser machining to form linear grooves and the grooves exhibit basic features of contact guidance for cell growth.

In our previous work, the Ti-20Zr-10Nb-4Ta alloy was found exhibiting good mechanical properties as well as shape memory effect [14]. In the present work, a focused laser surface treatment has been performed on the Ti-20Zr-10Nb-4Ta. The effects of laser surface treatment on the corrosion resistance and cytocompatibility were investigated.

MATERIALS AND METHODS

Materials

The Ti–20Zr–10Nb–4Ta (at.%, TZNT) alloy was prepared using high-purity (>99.9 wt.%) raw materials. The ingots (approximately 1.5 kg in weight) were re-melted five times for homogeneity *via* the non-consumable arc-melting method under Ar protection. The as-melted ingots were homogenized at 1237 K for 6 h in a vacuum of 10^{-3} Pa, cut into 4 mm thick pieces, and then cold rolled into sheets with 75% reduction in thickness. Next, alloy sheets were annealed at 873 K in vacuum for 30 min and quenched in water.

The sheets were cut into 11 mm×11 mm for experimentation. Before the laser ablation, the sample surface was ground by a series of sandpapers from 240 to 1500 grit and electropolished to a mirror. Then the samples were cleaned ultrasonically in methanol for 10 min, rinsed in distilled water for another 10 min, and dried thoroughly in cold air stream.

Laser ablation

The laser surface ablation process was performed using a pulsed wave 15 W fibre laser (PicoYL-15-0.1). The wavelength of the laser is 1064 nm, and the spot size is 35 μm. After cleaned with methanol and dried in air, the samples were irradiated with the fibre laser using the following processing parameters: laser power: 11.4 W, workpiece scanning speed: 700 mm s^{-1}, frequency: 100 kHz, shielding gas type: high purity argon. The Ar gas was delivered to the laser-irradiated area *via* side gas jets.

Surface topography and chemical composition

Images of the laser-treated TZNT surfaces were obtained with a scanning electron microscope. The surface profiles were determined using a white light interferometer. Changes in the chemical states and compositions of the surfaces in the depth direction were analyzed by X-ray photoelectron spectroscopy (XPS), using monochromatic Al Kα radiation. The spot size was 500 μm and the pass energy was set to 100.0 eV and 30.0 eV for wide spectrum and narrow spectrum scan analysis, respectively. The XPS measurements were measured at the surface of samples without any sputtering.

Contact angle and corrosion tests

To investigate the wetting properties of surface treated by laser, contact angle measurements were conducted for the laser treated and untreated samples using distilled water within two hours after sample processing. Electrochemical tests were conducted to evaluate the corrosion resistance ability of the untreated and laser treated samples in Hank's solution at a pH of 7.4. The composition of the Hank's solution included 8.00 g L^{-1} NaCl, 0.14 g L^{-1} CaCl, 0.40 g L^{-1} KCl, 0.10 g L^{-1} $MgCl_2{\cdot}6H_2O$, 0.10 g L^{-1} $MgSO_4{\cdot}7H_2O$, 0.35 g L^{-1} $NaHCO_3$, 0.12 g L^{-1} $Na_2HPO_4{\cdot}12H_2O$, 0.06 g L^{-1} KH_2PO_4 and 1.00 g L^{-1} Glucose. Potentio-dynamic polarization tests were carried out using a standard three-electrode system at the temperature of 37 ± 0.5°C and scan rate of 1 mV s^{-1}, which had a saturated calomel electrode as the reference electrode and a carbon electrode as the counter electrode. The test potential ranged below the open circuit potential of 300 mV to above that of 300 mV, and scanned from low potential to high potential. Exposed area of each sample was 1.21 cm^2. Polarization measurements started after the samples were immersed in the Hank's solution for 20 min under open-circuit conditions. Beyond that, the open circuit potential curves were measured for 12 h to obtain stable datum.

Evaluation of cellular response

MC3T3-E1 cells were cultured in α-modified minimum essential medium (α-MEM) containing 10% fetal bovine serum (FBS) and 1% of antibiotic–antimycotic solution at 37°C under a humidified atmosphere of 5% CO_2. The TZNT plates were sterilized with the ultraviolet lamp. Each sterilized TZNT plate was placed in a single well of a 12-well polystyrene cell-culture plate. The MC3T3-E1 cells were seeded within each well at a concentration of 1 × 10^4 cells mL^{-1} and then incubated for 12, 24 or 72 h. Morphological analysis of the cells was then performed using SEM. To prepare specimens for SEM analysis, the cells were washed three times in PBS (5 min each time), fixed with 2.5% glutaraldehyde under the condition of avoiding light for 1 h and rinsed in PBS again. Then the cells were dehydrated in sequential concentrations of

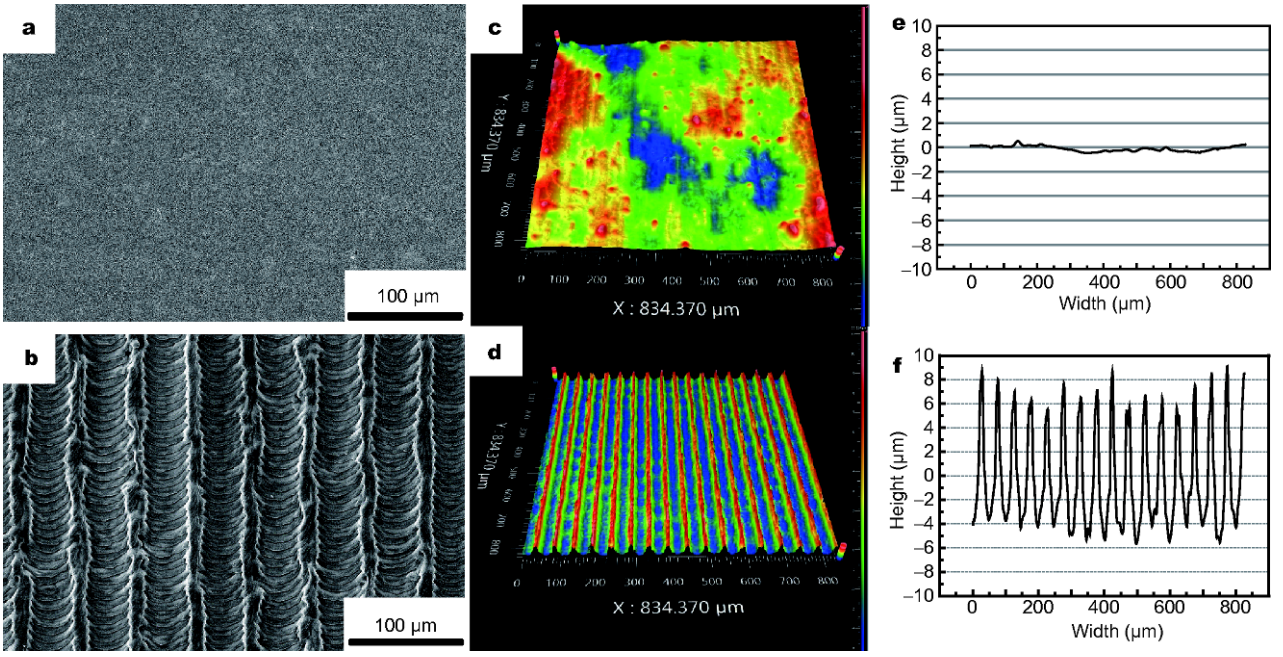

Figure 1 The surface images obtained by SEM: (a) untreated TZNT, (b) laser-treated TZNT surface. 3D surface profiles by optical measurement system: (c) untreated TZNT, (d) laser-treated TZNT. Surface undulation in a line by optical measurement system: (e) untreated TZNT, (f) laser-treated TZNT.

ethanol of 30%, 50%, 70%, 90% and 100% (15 min each concentration). The hexamethyl disilylamine was added for 15 min and then dried in air. After culturing, MTT assay was used to evaluate cell proliferation. The absorbance was measured at a wavelength of 492 nm on the enzyme-link meter.

Statistical analysis

All the results are presented as the means ± standard error of the mean. The data were statistically analyzed using the software program SPSS. One-way ANOVA with Duncan's multiple range test was used to examine differences between the groups. Values of $p<0.05$ were considered significant unless stated otherwise. Data from all experiments are representative from one of at least three repeated experiments.

RESULTS AND DISCUSSION

Surface characteristics

Fig. 1 shows the surface topography images of the untreated and laser-treated TZNT samples obtained by SEM and optical measurement system. It is seen in Fig. 1a that the untreated sample is smooth on the surface. However, the surface of the laser-treated sample is covered by rougher groove morphologies (Fig. 1b). It is noted that uniform ripples are observed at the bottom of the grooves. The width of the groove is about 40 μm, which is slightly larger than the diameter of the laser beam, 35 μm. The spacing distance of grooves is about 50 μm, which is almost the same as the distance of laser beam. The 3D surface profile of the untreated sample displays a roughness average (Ra) value of 0.202 μm as shown in Fig. 1c. A much higher Ra value of 4.175 μm was measured by the 3D surface profile of the laser treated TZNT in Fig. 1d, and corresponding depth of grooves is about 10 μm as shown in Fig. 1f. It is known that the micro-grooves with stripes are typical topographic features of laser-ablated samples. Mukherjee *et al.* [22] found that the laser ablation induced micro-grooves and ripples on the laser treated Ti-6Al-4V were dependent on the laser scanning parameters and, moreover, influenced the cellular activities and enhanced the biocompatibility.

Surface wettability

Fig. 2 shows the water contact angles of the laser-treated and untreated TZNT surfaces. It is seen that all the contact angles of the samples remain below 40°. The average water contact angle of untreated TZNT is isotropic and determined as 36.9°. In contrast, the laser treated TZNT exhibits obviously anisotropic contact angle. For the P direction, the average water contact angle is

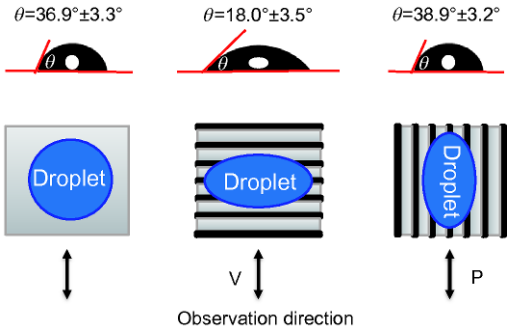

Figure 2 The water contact angles of the laser-treated and untreated TZNT surfaces.

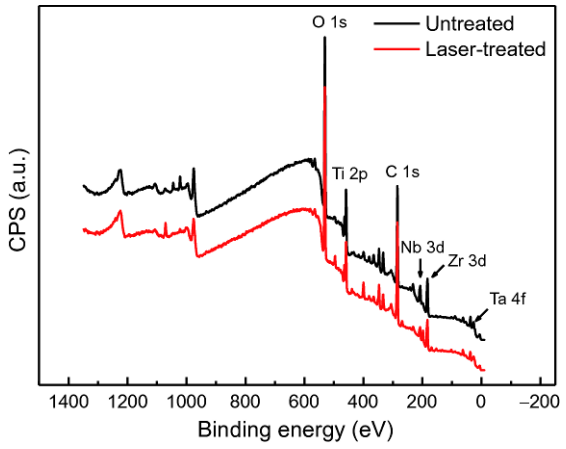

Figure 3 The XPS full spectra of untreated and laser-treated TZNT surface.

38.9° which is close to that of the untreated samples. For the V direction, the average water contact angle is 18.0°, which is about 51% lower than that of the untreated samples. Similar results have been found on laser treated Ti-6Al-4V alloy that the contact angle measured perpendicular to the orientation of the grooves was very different from that parallel to the grooves [22,23].

Surface chemical composition

Fig. 3 shows the XPS spectra of the untreated and laser-treated TZNT surface. It can be seen that apart from the presence of the expected key elements (Ti, Zr, Nb, Ta and O), both laser-treated and untreated surfaces reveal the presence of carbon (C). It was believed that carbon was present as a contamination from environment or cleaning process [24]. A summary of different elements detected in the outmost oxide layers on the laser-treated and untreated surfaces is given in Table 1. The quantitative compositional results indicate that the oxide film is enriched with more non-metallic elements (O and C) after laser surface treatment. The relative concentration of non-metallic elements in the outermost surface layer increases. In addition, the higher O concentration of untreated samples is owing to the electrobrightening which can form an oxide layer on the surface.

Fig. 4 shows the XPS spectra of different elements obtained from narrow scans over the Ti 2p, Nb 3d, Zr 3d, and Ta 4f lines for the laser-treated and untreated TNZT samples. The Ti 2p XPS spectra (Fig. 4a) of the untreated surface shows that the outermost oxide layer is mainly composed of TiO_2 (or Ti^{4+}), and small amounts of metallic Ti is also found. However, the laser-treated surface contains only TiO_2 without metallic Ti. The Zr 3d XPS spectrum (Fig. 4b) of the untreated surface shows that outermost oxide layer contains the Zr^{4+} and some metallic Zr. In comparison, the outermost oxide layer on the laser-treated surface is composed of Zr^{4+} and fewer metallic Zr. For Nb in the surface as seen in Fig. 4c, it is noted that Nb^{5+} peaks exist in both of the sample before and after leaser treatment, while the peak of 5/2 Nb^0 almost disappears after laser treatment. Ta oxide is characterized by Ta^{5+} peaks in the sample, which is independent to the laser treatment. These results indicated that the leaser treatment promoted the oxidation of Ti, Zr and Nb on the surface of the TZNT alloy, although high purity argon was used to protect the surface of the sample. Similar result has been found in Chan's study that a complete Nb oxide was found in the outermost layer on the laser-treated Ti-35.3Nb-7.3Zr-5.7Ta alloy and no other suboxides were detected [24].

Corrosion properties

Fig. 5a demonstrates the open circuit potential curves of the untreated and laser-treated TZNT samples in Hank's solution at 37°C. The steady values of OCPs of the samples are listed in Table 2. An obvious result can be obtained from Fig. 5a that the OCP of laser-treated TZNT

Table 1 The element content on TZNT surface with and without laser ablation

Element	O	Ti	Zr	Nb	Ta	C
Untreated (at.%)	38.47	6.21	3.70	1.69	0.69	49.24
Laser-treated (at.%)	35.56	4.80	2.90	1.11	0.41	55.22

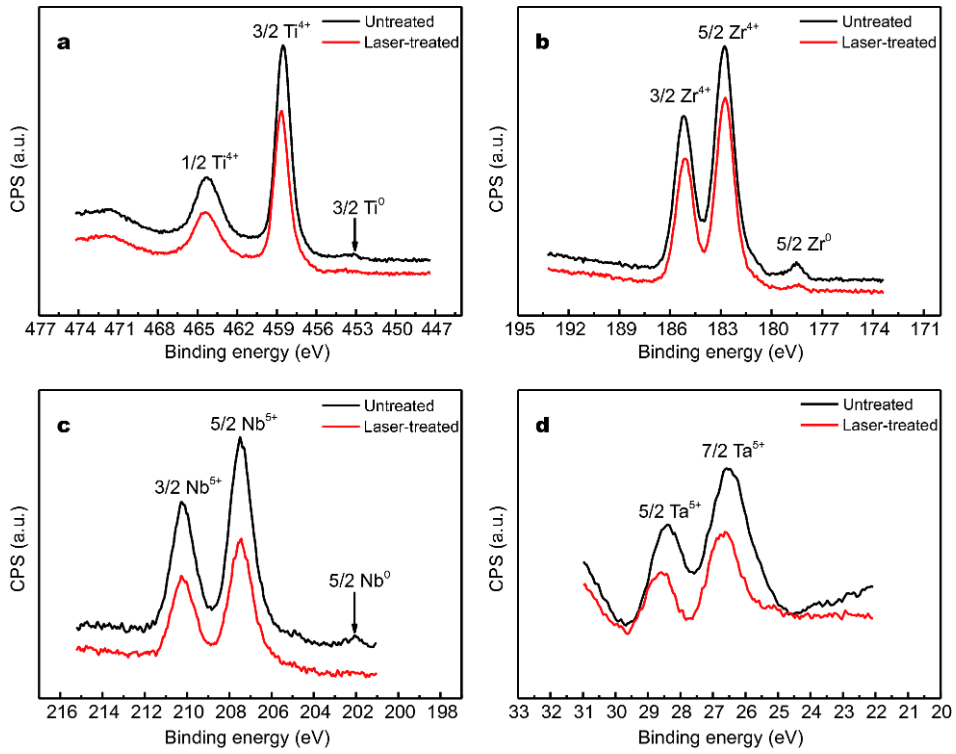

Figure 4 The XPS narrow spectra of (a) Ti, (b) Zr, (c) Nb and (d) Ta on the surface of untreated and laser-treated sample.

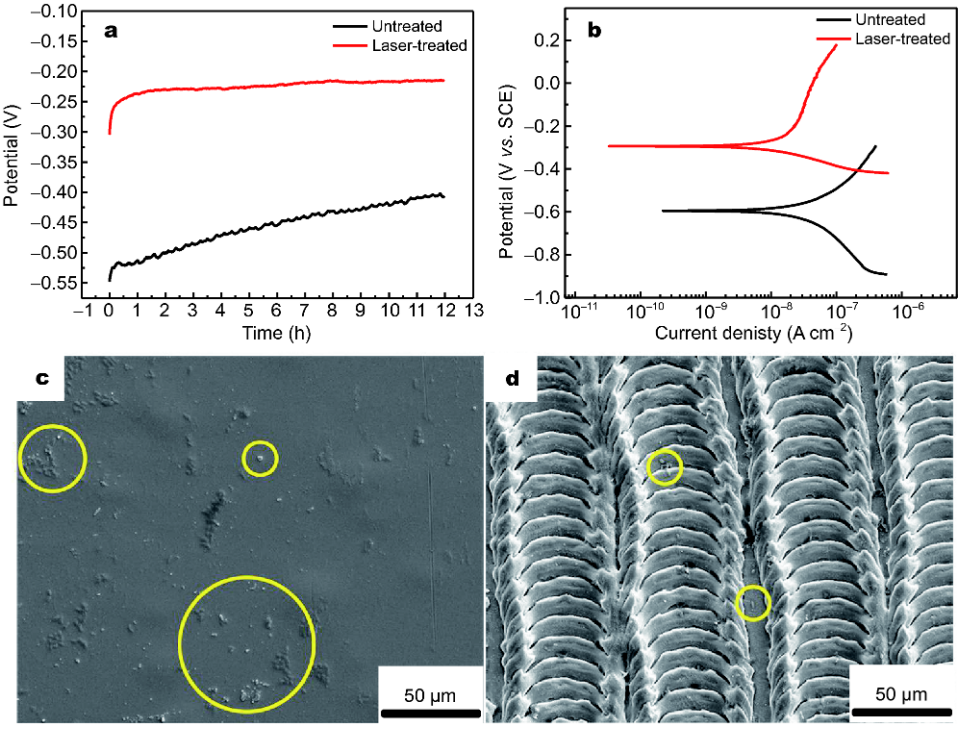

Figure 5 The open circuit potential curves (a) and the potentio-dynamic polarization curves (b) of untreated and laser-treated TZNT samples in Hank's at 37°C. (c, d) The SEM images of untreated and laser-treated samples after potentio-dynamic polarization test in Hank's at 37°C. The regions marked by yellow circle contain the corrosion products.

Table 2 The open circuit potentials (OCP), corrosion potentials (E_{corr}), corrosion current densities (i_{corr}) and polarization resistance (R_p) of untreated and laser-treated samples in Hank's at 37°C

Sample	OCP (mV)	E_{corr} (mV)	i_{corr} (A cm^{-2})	R_p (Ω cm^2)
Untreated	−405.68	−609.85	3.70×10^{-8}	1.20×10^6
Laser-treated	−214.82	−304.55	1.04×10^{-8}	2.26×10^6

is much higher than that of the untreated TZNT. A higher OCP indicates the formation of a thicker passivation layer [25,26]. The higher OCP of laser-treated TZNT indicates that laser-treated TZNT sample surface is more chemically stable compared to untreated TZNT. XPS analysis results can interpretate the changes of curves from Fig. 5a that the surfaces of untreated samples contain more metallic Ti, Zr and Nb compared with laser-treated samples.

Fig. 5b displays the potentio-dynamic polarization curves of the untreated and laser-treated TZNT samples in Hank's solution at 37°C. Fig. 5c, d show the surface morphology images of the untreated and laser-treated TZNT samples after potentio-dynamic polarization test in Hank's solution at 37°C. Table 3 shows the corrosion potential (E_{corr}) and corrosion current density (i_{corr}) of the TZNT in this work and those of laser treated Ti-6Al-4V [27] and Ti-35.3Nb-7.3Zr-5.7Ta [24] alloys. It is seen that the E_{corr} of the laser-treated TZNT samples increases by more than 300 mV. The i_{corr} of the laser-treated TZNT samples is obvious lower than that of the untreated sample regardless of the increased surface area of laser-treated samples. The corrosion products of untreated samples are significantly more than that of laser-treated samples. These results reveal a significant improvement in corrosion resistance of TZNT alloy after laser ablation. According to the XPS analysis, it is found that the laser treatment promoted the surface oxidation of TZNT alloy. Therefore, it is believed that the improved corrosion resistance measured in the polarization tests is due to the formation of more protective oxide film on the metal surface after laser ablation. Similar results have been found in Ti-6Al-4V [27] and Ti-35.3Nb-7.3Zr-5.7Ta [24] alloys. The increase in corrosion potential of laser-treated Ti-6Al-4V was possibly due to the presence of oxide as well as formation of refined microstructure and microstructural homogenization [27]. The laser-formed TiO_2/Nb_2O_5 layer on the surface of Ti-35.3Nb-7.3Zr-5.7Ta was contributed to the improved corrosion resistance of the alloy [24].

Cellular attachment and proliferation

Fig. 6 shows the MTT assay of MC3T3-E1 cells attached on the TZNT for 12, 24 and 72 h culture. It is seen that the cell number increases with increasing culture time for both of the samples. The cell number of laser-treated sample is slightly higher than that of the untreated samples at 12 or 24 h culture time. Therefore, the laser-treated TZNT alloy shows a positive effect on cell proliferation. Liang *et al.* [28] created several grooved morphologies on NiTi alloy surface by a femtosecond laser and the cell proliferation rate was found increasing with the increasing culture time due to the modification of the surface oxide with the reduction of Ni content. In addition, it was reported that the formation of a stable TiO_2 layer on a Ti substrate through anodic oxidation suppressed the adsorption of surface contaminants, leading to an improved surface hydrophilicity and enhanced cellular adhesiveness [29]. No significant differences in cell proliferation are found between the laser-treated and untreated samples after 72 h culture.

Fig. 7 shows the morphology of MC3T3-E1 cells on the untreated and laser-treated samples after 12, 24 and 72 h culture. It can be seen that the cells grew up, spread, contacted and fused gradually with increasing culture time for both of the untreated samples and laser-treated samples. It is seen in Fig. 7a that the MC3T3-E1 cells on the untreated samples exhibited oval and fusiform morphologies after 12 h culture. The filopodia of cells adhered to the surface of samples irregularly. It can be

Table 3 The corrosion potentials (E_{corr}) and corrosion current densities (i_{corr}) of Ti-20Zr-10Nb-4Ta, Ti-6Al-4V and Ti–35.3Nb–7.3Zr–5.7Ta alloys

Alloy composition	Sample	E_{corr} (mV)	i_{corr} (A cm^{-2})
Ti-20Zr-10Nb-4Ta	Untreated	−609.85	3.70×10^{-8}
	Treated	−304.55	1.04×10^{-8}
Ti-6Al-4V [27]	Untreated	−614	/
	Treated	−335	/
Ti–35.3Nb–7.3Zr–5.7Ta [24]	Untreated	−590	0.01507
	Treated	−431	0.00028

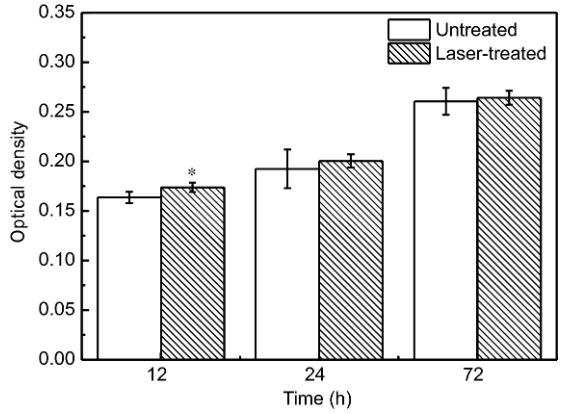

Figure 6 The MTT assay of MC3T3-E1 cells cultured for 12, 24 and 72 h on the untreated and laser-treated TZNT alloys. (* indicates significant difference compared with untreated TZNT (p<0.05).)

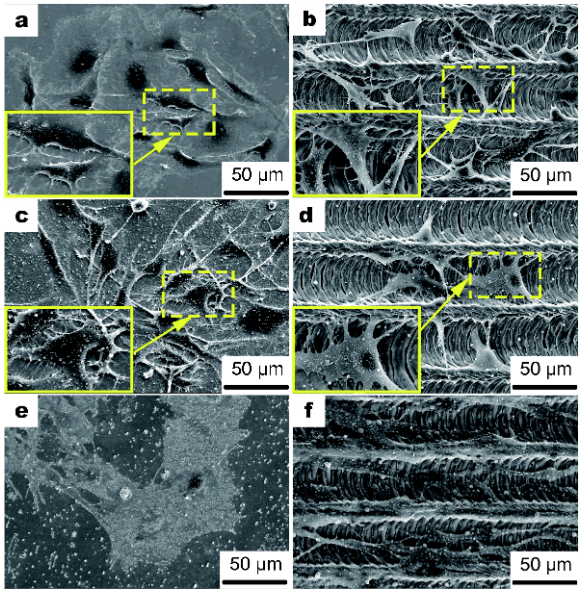

Figure 7 The SEM images of MC3T3-E1 cells cultured on the untreated TZNT alloys for 12 (a), 24 (c) and 72 h (e), and on the laser-treated TZNT alloys for 12 (b), 24 (d) and 72 h (f). The regions enclosed by yellow line represent the high magnification image.

seen in Fig. 7b that the most of the cells on laser-treated samples after 12 h culture displayed triangular shape with filopodia attached on the ridge of grooves. The phenomenon can be observed explicitly in the high magnification image identified with a yellow imaginary line. For the untreated sample after 24 h culture as show in Fig. 7c, the cells grew up in size, and the filopodia of cells begun bonding each other. Moreover, cells on the laser treated sample after 24 h culture produced more filopodia attached on the ridge (see Fig. 7d). When the culture time reached 72 h, it is observed in Fig. 7e that the cells on the untreated sample were completely fused and grew laminated. These results indicated that more and more connections between filopodia of cells occurred with the increasing incubation time. It can be observed in Fig. 7f that most of the cells on the laser treated sample after 72 h culture exhibit shuttle-like shape distributed along the groove direction. This indicates that the growth of attached MC3T3-E1 cells was definitely guided by the anisotropic groove morphology as well as the reduction of water contact angle along the groove direction. Similar results have been found on a laser treated Ti-6Al-4V surfaces, on which the direction of microgrooves and nanostructures controlled the cell alignment regularly, and the cells grew along the groove primarily [30]. Based on the results of cell culture experiments, it can be concluded that laser ablation improved the surface biocompatibility because of the formation of more stable oxide layer and improved corrosion resistance. Moreover, the micro-grooves not only guide the cell growth, but also provide more surface area in comparison to the untreated surfaces, which was favorable for protein adsorption, resulting in improved biocompatibility [22,28].

CONCLUSIONS

The corrosion behavior and cytocompatibility of Ti–20Zr–10Nb–4Ta alloy have been investigated and the following conclusions were reached. The laser treatment caused rougher groove morphologies on the surface of the Ti–20Zr–10Nb–4Ta alloy and promoted the oxidation of Ti, Zr and Nb elements. The corrosion resistance of the alloy was improved by laser treatment as evidenced by an enhanced corrosion potential from −609.85 to −304.55 mV and a reduced corrosion current density from 3.70×10^{-8} to 1.04×10^{-8} A cm^{-2} in the anodic polarization test in Hank's solution. The laser-treated Ti–20Zr–10Nb–4Ta alloy showed similar cell viability compared with the untreated alloy. Moreover, more hydrophilic surface and presence of the anisotropic groove pattern induced obvious orientation for cell growth.

Received 5 November 2017; accepted 5 March 2018; published online 21 March 2018

1 Deligianni D. Effect of surface roughness of the titanium alloy Ti–6Al–4V on human bone marrow cell response and on protein adsorption. Biomaterials, 2001, 22: 1241–1251
2 Scarano A, Piattelli M, Caputi S, *et al.* Bacterial adhesion on commercially pure titanium and zirconium oxide disks: an *in vivo* human study. J Periodontol, 2004, 75: 292–296
3 El-Ghannam A, Starr L, Jones J. Laminin-5 coating enhances epithelial cell attachment, spreading, and hemidesmosome as-

sembly on Ti-6Al-4V implant material *in vitro*. J Biomed Mater Res, 1998, 41: 30–40
4 Niinomi M, Nakai M, Hieda J. Development of new metallic alloys for biomedical applications. Acta Biomater, 2012, 8: 3888–3903
5 Hao YL, Li SJ, Yang R. Biomedical titanium alloys and their additive manufacturing. Rare Met, 2016, 35: 661–671
6 Qu WT, Sun XG, Yuan BF, *et al.* Tribological behaviour of biomedical Ti–Zr-based shape memory alloys. Rare Met, 2017, 36: 478–484
7 Jin M, Lu X, Qiao Y, *et al.* Fabrication and characterization of anodic oxide nanotubes on TiNb alloys. Rare Met, 2016, 35: 140–148
8 Oliveira NTC, Ferreira EA, Duarte LT, *et al.* Corrosion resistance of anodic oxides on the Ti–50Zr and Ti–13Nb–13Zr alloys. Electrochim Acta, 2006, 51: 2068–2075
9 Elias LM, Schneider SG, Schneider S, *et al.* Microstructural and mechanical characterization of biomedical Ti–Nb–Zr(–Ta) alloys. Mater Sci Eng-A, 2006, 432: 108–112
10 Fukuda A, Takemoto M, Saito T, *et al.* Bone bonding bioactivity of Ti metal and Ti–Zr–Nb–Ta alloys with Ca ions incorporated on their surfaces by simple chemical and heat treatments. Acta Biomater, 2011, 7: 1379–1386
11 Ozan S, Lin J, Li Y, *et al.* New Ti-Ta-Zr-Nb alloys with ultrahigh strength for potential orthopedic implant applications. J Mech Behav BioMed Mater, 2017, 75: 119–127
12 Xue P, Li Y, Li K, *et al.* Superelasticity, corrosion resistance and biocompatibility of the Ti–19Zr–10Nb–1Fe alloy. Mater Sci Eng-C, 2015, 50: 179–186
13 Xiong C, Xue P, Sun B, *et al.* Effect of annealing temperature on the microstructure and superelasticity of Ti-19Zr-10Nb-1Fe alloy. Mater Sci Eng-A, 2017, 688: 464–469
14 Xiong C, Yao L, Yuan B, *et al.* Strain induced martensite stabilization and shape memory effect of Ti–20Zr–10Nb–4Ta alloy. Mater Sci Eng-A, 2016, 658: 28–32
15 Soboyejo WO, Nemetski B, Allameh S, *et al.* Interactions between MC3T3-E1 cells and textured Ti6Al4V surfaces. J Biomed Mater Res, 2002, 62: 56–72
16 Ohtsu N, Kozuka T, Yamane M, *et al.* Surface chemistry and osteoblast-like cell response on a titanium surface modified by a focused Nd:YAG laser. Surf Coatings Tech, 2017, 309: 220–226
17 Man HC, Cui ZD, Yue TM. Corrosion properties of laser surface melted NiTi shape memory alloy. Scripta Mater, 2001, 45: 1447–1453
18 Wong MH, Cheng FT, Pang GKH, *et al.* Characterization of oxide film formed on NiTi by laser oxidation. Mater Sci Eng-A, 2007, 448: 97–103
19 Lawrence J, Hao L, Chew HR. On the correlation between Nd:YAG laser-induced wettability characteristics modification and osteoblast cell bioactivity on a titanium alloy. Surf Coatings Tech, 2006, 200: 5581–5589
20 Chen J, Ulerich JP, Abelev E, *et al.* An investigation of the initial attachment and orientation of osteoblast-like cells on laser grooved Ti-6Al-4V surfaces. Mater Sci Eng-C, 2009, 29: 1442–1452
21 Ulerich JP, Ionescu LC, Chen J, et al. Modifications of Ti-6Al-4V surfaces by direct-write laser machining of linear grooves. Proc of SPIE, 2007, 6458: 645819
22 Mukherjee S, Dhara S, Saha P. Enhancing the biocompatibility of Ti6Al4V implants by laser surface microtexturing: an *in vitro* study. Int J Adv Manuf Technol, 2015, 76: 5–15
23 Raimbault O, Benayoun S, Anselme K, *et al.* The effects of femtosecond laser-textured Ti-6Al-4V on wettability and cell response. Mater Sci Eng-C, 2016, 69: 311–320
24 Chan CW, Lee S, Smith G, *et al.* Enhancement of wear and corrosion resistance of beta titanium alloy by laser gas alloying with nitrogen. Appl Surf Sci, 2016, 367: 80–90
25 Saebnoori E, Shahrabi T, Sanjabi S, *et al.* Surface characteristics and electrochemical behaviour of sputter-deposited NiTi thin film. Philos Mag, 2015, 95: 1696–1716
26 Li K, Li Y, Huang X, *et al.* Surface microstructures and corrosion resistance of Ni-Ti-Nb shape memory thin films. Appl Surf Sci, 2017, 414: 63–67
27 Kumari R, Scharnweber T, Pfleging W, *et al.* Laser surface textured titanium alloy (Ti–6Al–4V) – Part II – Studies on bio-compatibility. Appl Surf Sci, 2015, 357: 750–758
28 Liang C, Wang H, Yang J, *et al.* Biocompatibility of the micropatterned NiTi surface produced by femtosecond laser. Appl Surf Sci, 2012, 261: 337–342
29 Ohtsu N, Kozuka T, Hirano M, *et al.* Electrolyte effects on the surface chemistry and cellular response of anodized titanium. Appl Surf Sci, 2015, 349: 911–915
30 Dumas V, Rattner A, Vico L, *et al.* Multiscale grooved titanium processed with femtosecond laser influences mesenchymal stem cell morphology, adhesion, and matrix organization. J Biomed Mater Res, 2012, 100A: 3108–3116

Acknowledgements This work was supported by the National Natural Science Foundation of China (NSFC, 51771011) and the Fundamental Research Funds for the Central Universities (KG12002601).

Author contributions Xue X conceived and designed the experiments, analyzed the results, and wrote the manuscript. Ma C prepared the samples and participated in the characterization; An H involved in the paper writing and experiments designing; Li Y and Guan Y supervised the experiments designing and paper writing. All authors contributed to the general discussion.

Conflict of interest The authors declare that they have no conflict of interest.

Xianda Xue received his bachelor's degree from Beihang University in 2014. Now he is pursuing his PhD degree (metallic materials) at Beihang University continuously. His research interests focus on the technique improving surface of metallic materials.

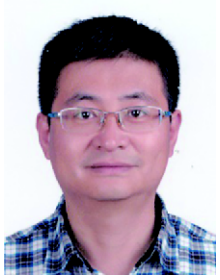

Yan Li is a professor of the School of Materials Science and Engineering at Beihang University. He received his PhD degree from Dalian University of Technology in 2001. His current research interests include shape memory materials, biomedical materials, and supercapacitors and battery materials.

Yingchun Guan is currently a professor in the School of Mechanical Engineering and Automation, Beihang University. She received her PhD degree from Nanyang Technological University (Singapore) in 2011. She had been served as Scientist in Singapore Institute of Manufacturing Technology from 2011 to 2014. Her major research interests include laser precision manufacturing and laser additive manufacturing.

激光表面改性Ti-20Zr-10Nb-4Ta合金的耐腐蚀性与细胞相容性研究

薛贤达[1], 马程鹏[2], 安红娟[1], 李岩[1,3*], 管迎春[2,4,5*]

摘要 本文系统研究了激光表面改性对Ti-20Zr-10Nb-4Ta(TZNT)合金耐腐蚀性和细胞相容性的影响. 扫描电镜观察结果表明, 激光改性能够在TZNT合金表面制造沟槽结构, 沟槽宽度大概40 μm, 沟槽深度大概10 μm. 与未处理样品相比, 改性样品表面沿沟槽方向的水接触角减小了51%. 激光处理过程使样品表面金属态的Ti、Zr和Nb转变成了稳定的氧化态. 在37°C的Hank's溶液中进行动电位极化测试发现, 改性样品的自腐蚀电位升高了50%, 自腐蚀电流密度下降了72%, 说明激光改性能够提高TZNT合金的耐腐蚀能力. MTT实验结果表明小鼠成骨细胞(MC3T3-E1)在改性样品和非改性样品表面具有相似的细胞活性. 从细胞形貌可以看出, 细胞出现了沿沟槽方向生长的导向性. 综上所述, 新型生物医用TZNT合金有望成为骨科和牙科植入领域的替代材料.

